Mathematical Modelling and Feasibility Study of the Biomimetic Undulating Fin of a Knife Fish Robot

Submitted: 27th August 2015; accepted 9th November 2015

Ajith Anil Meera, Attadappa Puthanveetil Sudheer

DOI: 10.14313/JAMRIS_1-2016/3

Abstract:
Bio-mimetic underwater robotics is an emerging area of research, which has the potential to substitute the conventional energy inefficient mode of underwater propulsion using thrusters. In this paper, the mathematical modelling of the undulating fin is done and the effect of various parameters of the mechanism design on the available workspace is studied. The mathematical beauty is revealed, for the curves representing the mechanical constraint and the family of undulating waves. The feasibility of a wave to be generated by the mechanism was analyzed.

Keywords: *biomimetic design, propulsion, fins, mechanism, underwater robotics, five bar mechanism, fish robot*

1. Introduction

Nature provides us the best and robust solutions for underwater propulsion through living organisms under water subjected to evolutionary optimization. This notion has made man enthusiastic about observing the marine life and replicating it in the underwater vehicles. This has opened up a new realm for research called bio-mimetic underwater robotics. As a result, wide range of underwater robots were designed and tested for better propulsive efficiency around the globe. Nanyang Technological University's NKF-1 Knife fish robot, Squid type vehicle from Osaka University, MIT's Robotuna, Festo's Airacuda and Stingray robot are some of them.

Number of papers have been published based on these works. The experimental results and conclusions of the swimming knife fish robot with undulating fin is dealt in [1], while the hydrodynamic analysis and forward thrust estimation for the robot propelled by two undulating side fins is discussed in [2]. The empirical results of braking performance of the two undulating side fin robot is done in [3], while the efficiency of usable area of a mechanism was quantified in [4]. The modelling of the motion of a biomimetic underwater vehicle was done in [5].

Developments in the field of experimental biology have expedited the growth of bio-mimetic robots. The experimental results for hovering and swimming of electric ghost knife fish, which could be used to mimic the real fishes is done in [6]. The disturbances and fluid patterns caused by the undulating fin under water is discussed in [7] and [8]. The role of counter propagation waves used by fishes for propulsion and maneuverability is revealed in [9] and [10]. However, the above literature does not explore the modelling and parametric study of the fin mechanism in depth. In this paper, the mathematical model of the fin mechanism is formulated and the feasibility of the waves to be generated by the mechanism is studied. The robot was tested for different waveforms and was found to make a smooth and eco-friendly swimming along with the real fishes.

2. Mechanism

The fin mechanism consist of a series of five bar mechanism with the non-crank member as a slider or a flexible membrane as introduced in [1].

2.1. Kinematic Design

The mechanism to generate a sinusoidal profile on the fin consists of cranks of length R placed at a fixed distance L between each other.

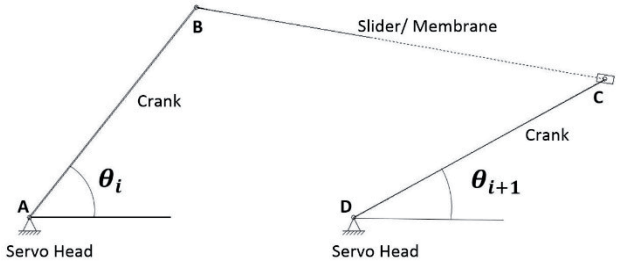

Fig. 1. Mechanism for sinusoidal wave generation

In Fig. 1, A and D represent the servo heads of the adjacent servo motors rotating about an axis perpendicular to the plane of the paper. Each of the cranks are made to move in a circular arc with the respective servo head as the center, as given in [4]. Intervals AB and DC represent the cranks of the servo motors and BC represents a mechanical slider. The angle θ made by the crank with the horizontal varies sinusoidal with respect to time. The phase difference between the adjacent crank angles is fixed as β. N number of servo motors are mounted with all the servo heads lying on the line joining A and D together creating an undulation on the fin. The equation of motion for ith crank is described by (1), where θ_m represents the maximum inclination of the cranks with the horizontal, f the frequency and t the time.

$$\theta_i = \theta_m \sin(2\pi f t + (i-1)\beta) \quad (1)$$

The fin is represented by the line joining the ends of the cranks. These lines represent the side view of the plane of the sliders kept between the crank ends. The ends of the cranks together impart a sinusoidal waveform to the fin. Hence each of the sliders kept between the crank ends, together form an approximate sine wave. The length of each slider varies as per the motion of the corresponding adjacent cranks.

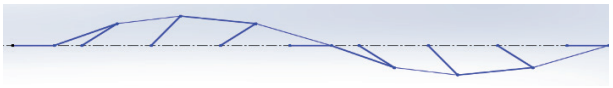

Fig. 2. Sinusoidal wave made by fin with N = 9, ϑm = 45° and β = 45° at t = 0 s

Fig. 2 represents the sketch of the sine wave generation by the fin mechanism, while Fig. 3 shows the undulating fin made using a stretchable membrane.

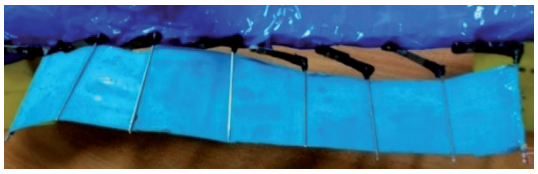

Fig. 3. Undulating fin with a flexible membrane

2.2 Mechanical Constraints:

The distance between the adjacent crank ends varies with respect to time. If the distance between the crank ends is less than a minimum value C_{min}, the slider hits. If the distance is more than the maximum value C_{max}, the slider detaches. Due to this mechanical constraint offered by the sliders, the distance between the crank ends are restricted to be within a range. The minimum and maximum stretchable lengths represents the mechanical constraint for a flexible membrane.

3. Parametric Study on Workspace:

The effect of parameter selection of the mechanism on the available workspace is studied in this section. The interdependency of the parameters is studied so that the mechanism can generate the sine waves.

3.1. Curves of Fixed Link Length

The workspace of the adjacent crank angle is a property of the mechanical design of the fin. The parameters affecting the workspace design are *L*, *R* and C_{min} and C_{max}. Proper selection of these parameters is essential to optimize the workspace. Since the servo motors are able to deliver –90° to 90° rotations with position control, the workspace design was done within a domain of $-\frac{\pi}{2} \le \theta_i \le \frac{\pi}{2}$ and $-\frac{\pi}{2} \le \theta_{i+1} \le \frac{\pi}{2}$ only.

Consider a five bar linkage represented by Fig. 1. with equal crank lengths and let the coupler BC be rigid with a fixed length C. From Fig. 1. the position of *B* at any time relative to A is $(R\cos\theta_i, R\sin\theta_i)$ and the position of *C* relative to A is $(L + R\cos\theta_{i+1}, R\sin\theta_{i+1})$. Evaluating the distance BC and equating it to *C* yields the expression given by (2), which on further simplification yields (3).

$$\left(\frac{C}{R}\right)^2 = \left(\cos\theta_i - \cos\theta_{i+1} - \frac{L}{R}\right)^2 + (\sin\theta_i - \sin\theta_{i+1})^2 \quad (2)$$

$$\left(\frac{L^2 - C^2}{R^2}\right) - 2\cos(\theta_i - \theta_{i+1}) - 2\left(\frac{L}{R}\right)\cos\theta_i + 2\left(\frac{L}{R}\right)\cos\theta_{i+1} + 2 = 0 \quad (3)$$

3.1.1. Taylor Series Approximation:

The Taylor series approximation was done on equation (3) and the powers higher of θ_i and θ_{i+1} were neglected, resulting in equation (4).

$$\theta_i^2\left(1 + \frac{L}{R}\right) + \theta_{i+1}^2\left(1 - \frac{L}{R}\right) - 2\theta_i\theta_{i+1} + \left(\frac{L^2 - C^2}{R^2}\right) = 0 \quad (4)$$

The error of approximation is dependent on *L/R* and independent of *C*. For different values of *L/R*, workspace plot for both (3) and (4) were plotted and was observed that the curves representing (4) completely lies inside the curves represented by (3) in the domain selected for analysis.

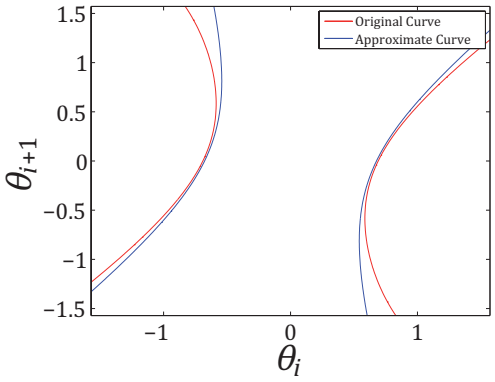

Fig. 4. Plot for L=5, R=3 and C=6

Moreover, the error was found to increase as the curve passes through points with either of the crank angles closer to 90° as shown in Fig. 4 (axes measured in radians). However, the approximated curves represent the original curve with a small error for the regions closer to the origin.

Since the approximated curves are always found to be inside the original curves, no point on the curve represented by equation (4) would violate the original mechanical constraint. Hence, replacing the original equation with an approximated equation is equivalent to offering more constraints to the workspace, without violating the original constraint at any point. The advantage of neglecting the higher order terms in the expansion of the cosine series is that it leads to a simple general form of a second degree polynomial curve with properties that can easily be analyzed through mathematical modelling. Hence, throughout the paper, the equation governing the adjacent crank angles was selected as given by equation (4).

3.1.2. Nature of the Curves

The curve represented by equation (4) is that of a general second degree equation of the form given by (5).

$$ax^2 + 2hxy + by^2 + 2gx + 2fy + c = 0 \qquad (5)$$

To determine the nature of the curve, two parameters Δ and D have to be evaluated, where

$$\Delta = \begin{vmatrix} a & h & g \\ h & b & f \\ g & f & c \end{vmatrix} \text{ and } D = h^2 - ab.\ \Delta = -\left(\frac{L}{R}\right)^2 \left(\frac{L^2 - C^2}{R^2}\right) \neq 0$$

$D = \left(\frac{L}{R}\right)^2 > 0$ and for (4). Hence, it can be concluded that if $L = C$, the equation (4) represents a pair of straight lines and if $L \neq C$ it represents the equation of a hyperbola.

3.1.3. Standard Form of Hyperbola

The equation (4) represents a family of hyperbola inclined to the axes for $L \neq C$. To formulate the standard equation of the hyperbola, the axes are rotated about an axis perpendicular to the paper such that the transformed axis is coincident with the major axis of the hyperbola, as shown in Fig. 5.

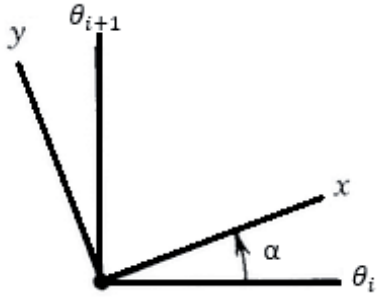

Fig. 5. Rotation about z axis

The transformation matrix for rotation about z-axis is represented by

$$\boldsymbol{T} = \begin{bmatrix} \cos\alpha & \sin\alpha & 0 \\ -\sin\alpha & \cos\alpha & 0 \\ 0 & 0 & 1 \end{bmatrix}.$$

Hence the transformation is represented by

$$\begin{bmatrix} x \\ y \\ 0 \end{bmatrix} = T \begin{bmatrix} \theta_i \\ \theta_{i+1} \\ 0 \end{bmatrix}$$

$$or \begin{bmatrix} \theta_i \\ \theta_{i+1} \\ 0 \end{bmatrix} = \boldsymbol{T}^{-1} \begin{bmatrix} x \\ y \\ 0 \end{bmatrix} = \begin{bmatrix} \cos\alpha & -\sin\alpha & 0 \\ \sin\alpha & \cos\alpha & 0 \\ 0 & 0 & 1 \end{bmatrix} \begin{bmatrix} x \\ y \\ 0 \end{bmatrix}.$$

Hence, the standard equation of the hyperbola is obtained after transformation as given by equation (6) for $C > L$ and equation (7) for $C < L$.

$$\frac{x^2}{\left(\frac{\left(\frac{C^2 - L^2}{R^2}\right)}{\sqrt{1 + \left(\frac{L}{R}\right)^2} + 1}\right)} - \frac{y^2}{\left(\frac{\left(\frac{C^2 - L^2}{R^2}\right)}{\sqrt{1 + \left(\frac{L}{R}\right)^2} - 1}\right)} = 1 \qquad (6)$$

$$\frac{x^2}{\left(\frac{\left(\frac{L^2 - C^2}{R^2}\right)}{\sqrt{1 + \left(\frac{L}{R}\right)^2} + 1}\right)} - \frac{y^2}{\left(\frac{\left(\frac{L^2 - C^2}{R^2}\right)}{\sqrt{1 + \left(\frac{L}{R}\right)^2} - 1}\right)} = -1 \qquad (7)$$

The hyperbolas represented by $C > L$ and $C < L$ have mutually perpendicular axis. Moreover, the curve represent a pair of straight lines at $C = L$.

The inclination of the transverse axis of the hyperbola with respect to the θ_i axis is represented by α, given by (8), which is dependent on L/R and is independent of C. The conjugate axis of the hyperbola is perpendicular to the transverse axis obtained.

$$\alpha = \frac{1}{2} tan^{-1}\left(-\frac{R}{L}\right) \qquad (8)$$

3.1.4. Asymptotes of the Hyperbola

The asymptotes of the hyperbola play a crucial role in the workspace design of the adjacent cranks. The equation representing the pair of asymptotes is given by (9).

$$\frac{\theta_{i+1}}{\theta_i} = 1 \; and \; \frac{\theta_{i+1}}{\theta_i} = \left(\frac{1 + \frac{L}{R}}{1 - \frac{L}{R}}\right) \qquad (9)$$

Hence, it can be concluded that the asymptotes are dependent on L/R and is independent of C. Moreover, $\theta_{i+1} = \theta_i$ is an asymptote which is independent of the

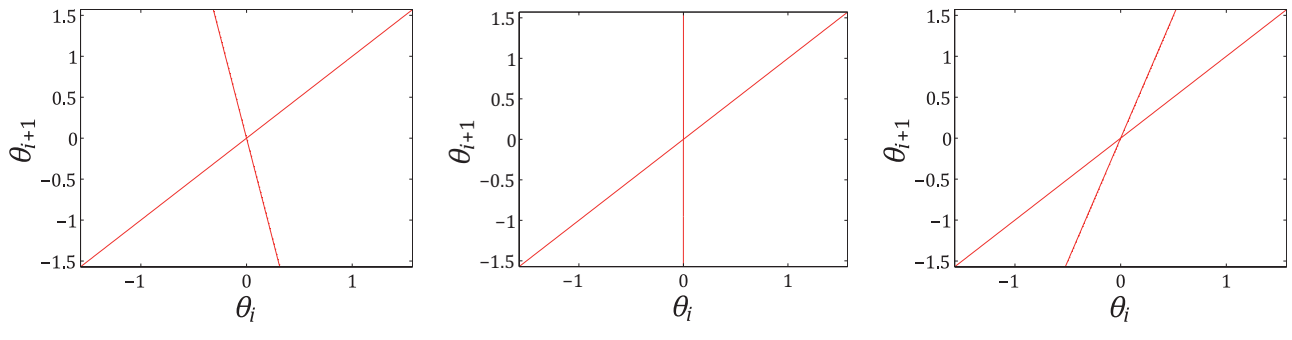

Fig. 6. Pair of asymptotes for L/R = 1.5, L/R = 1, L/R = 0.5, respectively

link lengths of the mechanism. The other asymptote is $\theta_i = 0$ for $L = R$. The asymptote has a negative slope for $L > R$ and a positive slope for $L < R$. Both the asymptotes pass through the origin for all cases. This result is illustrated in Fig. 6. The axes of all the graphs in the paper are measured in radians.

3.2. Workspace for Variable Link Length

Equation (4) represents the variation of the adjacent crank angles with equal crank lengths constrained to move with all the links of fixed length. Considering the non-crank member to be a membrane with $C_{min} \leq C \leq C_{max}$, and plotting all the intermediate curves yields a region corresponding to the workspace of the adjacent crank angles. The workspace is represented by an area bounded by the curves represented by equations (10) and (11) and is equivalent to relation (12).

$$\theta_i{}^2\left(1+\frac{L}{R}\right)+\theta_{i+1}{}^2\left(1-\frac{L}{R}\right)-2\theta_i\theta_{i+1} + \left(\frac{L^2-C_{min}{}^2}{R^2}\right)=0 \tag{10}$$

$$\theta_i{}^2\left(1+\frac{L}{R}\right)+\theta_{i+1}{}^2\left(1-\frac{L}{R}\right)-2\theta_i\theta_{i+1} + \left(\frac{L^2-C_{max}{}^2}{R^2}\right)=0 \tag{11}$$

$$\left(\frac{C_{min}}{R}\right)^2 \leq \theta_i{}^2\left(1+\frac{L}{R}\right)+\theta_{i+1}{}^2\left(1-\frac{L}{R}\right) - 2\theta_i\theta_{i+1}+\left(\frac{L}{R}\right)^2 \leq \left(\frac{C_{max}}{R}\right)^2 \tag{12}$$

It can be concluded that the area is defined by the region bounded by the boundary curves represented by (10) and (11). Hence, the workspace of the adjacent crank angles is defined as the area bounded by the boundary curves in the domain $\frac{\pi}{2} \leq \theta_i \leq \frac{\pi}{2}$ and $-\frac{\pi}{2} \leq \theta_{i+1} \leq \frac{\pi}{2}$. It represents the region in which the design of the lengths of the linkages constrain the motion of the adjacent crank angles. Increase in the workspace corresponds to a lesser constrain over the adjacent crank angles. Therefore, in order to increase the flexibility in the motion of the adjacent cranks, the workspace has to be optimized.

3.2.1. Parametric Study for the Workspace

It can be observed from (4) that the equation of the hyperbola defining the motion of the 4 bar linkage depends on two ratios, L/R and C/R. This implies that the hyperbola remains the same even if the mechanism is scaled up or down. This result allows to scale the mechanism in order to increase or decrease the size of the robot.

Parametric study for the hyperbola therefore constitutes a methodology involving the two ratios. Different cases of the parametric study are explored in which L/R is fixed and then C is varied covering all the possible ratio ranges. In the study, the L/R ratio is chosen to be either less than 1 or greater than 1. A feasible value for L and R is selected randomly such that the L/R falls in the selected range. The value of C is varied from a value less than min (L, R) to a value more than max (L, R). This results in three different cases of the range

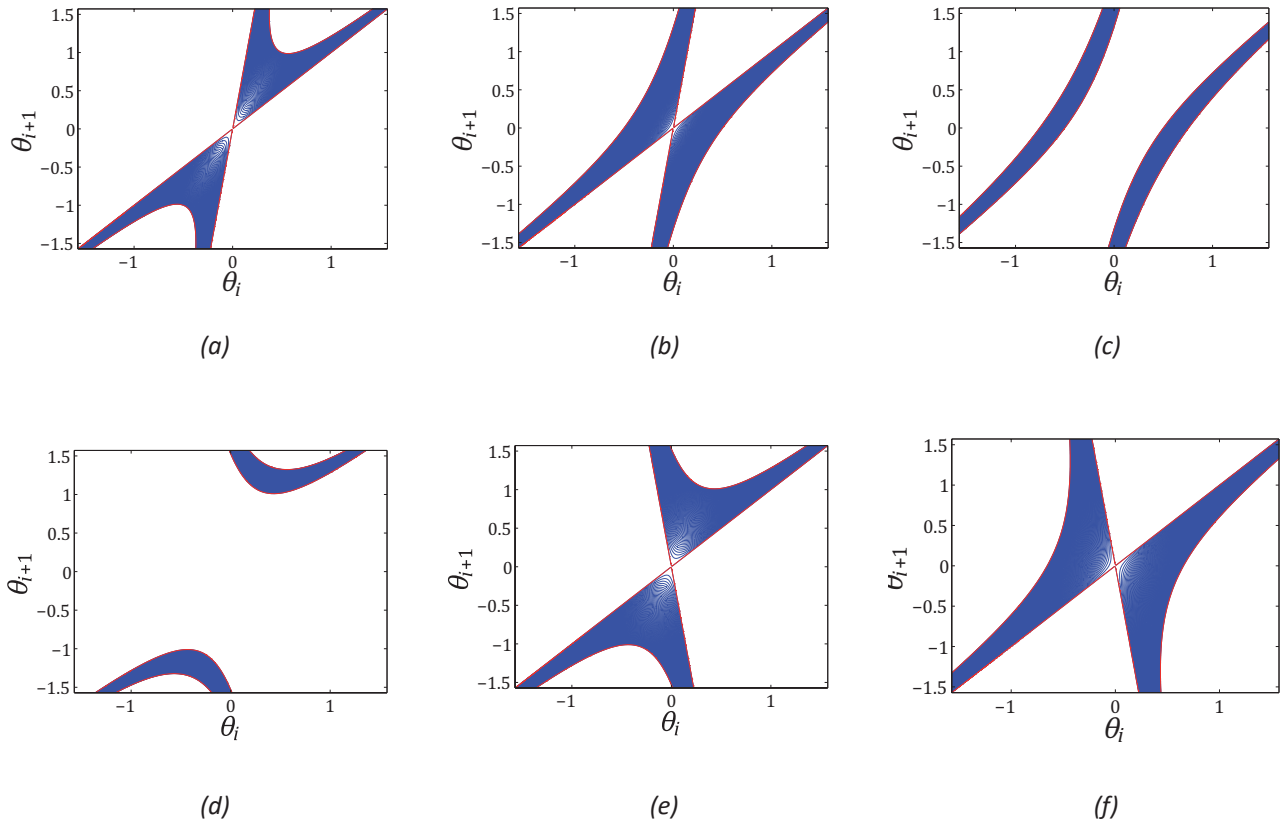

Fig. 7. Effect of parameter selection on workspace for L≠R

of C, excluding the condition of equality of C with L or R. The workspace plot for all the three cases were plotted. The three cases were repeated for the other range of L/R ratio.

Fig. 7(a, b, c) represents the 3 cases of the workspace for $\frac{L}{R}$. The parameters chosen were, L = 3, R= 4, C_{min} = 2 and C_{max} = 5. Fig. 7a: $C_{min} < C < L$, Fig. 7b: $L < C < R$, and Fig 7c: $R < C < C_{max}$. The asymptotes of the hyperbolas can be observed to be as in equation (8), and is independent of C. Both the asymptotes have a positive slope.

Fig. 7 (d, e, f) represents the three cases of the workspace for $\frac{L}{R} > 1$. The parameters chosen were, R = 3, L = 4, C_{min} = 2 and C_{max} = 5. Fig. 7d: $C_{min} < C < R$, Fig. 7e: $R < C < L$, Fig. 7f: $L < C < C_{max}$. The asymptotes of the hyperbolas can be observed to be as in equation (8), and is independent of C. One asymptote has a negative slope.

Fig. 7 represents the effect of selection of the slider properties on the total workspace of the mechanism for a chosen L and R. Therefore, the slider parameters have to be chosen such that the workspace is optimum. The transverse axis of the hyperbola changes beyond $C = L$, i.e. after Fig. 7a for $L < R$ and after Fig. 7e for $L > R$. It is in agreement with the results of the section 3.1.3. This property of the curve is crucial in the slider selection in the later section. The equality of C and R does not serve any characteristic property changes in the curves, while the equality of L and R give rise to different properties for $C < L$ and $C > L$.

Fig. 8 represents the two cases of the workspace for $L = R$, $C < L$ and $C > L$, respectively. The parameters selected were $L = R = 3$. The asymptotes are in agreement with the results of 3.1.3.

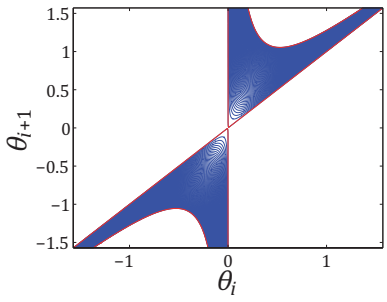

(a)

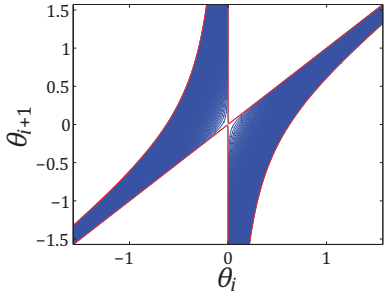

(b)

Fig. 8. Effect of parameter selection on workspace for L=R

Hence, it can be concluded that the asymptotes corresponding to the $\frac{L}{R}$ ratio divide the entire domain $-\frac{\pi}{2} \leq \theta_i \leq \frac{\pi}{2}$ and $-\frac{\pi}{2} \leq \theta_{i+1} \leq \frac{\pi}{2}$ into two regions, $\frac{C}{L} < 1$ and $\frac{C}{L} > 1$. The characteristic of the hyperbola in a region is its axis. The two regions have hyperbolas with axes mutually perpendicular to each other. The conjugate axis of hyperbolas in a region acts as the transverse axis in the other region and vice versa. The L/R ratio decides the inclination α of the transverse axis with the θ_i axis as discussed in 3.1.3. The region corresponding to a slider can fall in any of the two regions or both. Hence the selection of C_{min} and C_{max} determines the region in which the family of hyperbolas might belong.

4. Motion Planning for Undulation of Fins

The knife fish robot propels under water by creating an undulation of the anal fin through the controlled and combined motion of the servo motors kept in series along the fish body. The robot propagates through the generation of propagating sinusoidal waves of constant or linearly increasing amplitudes.

4.1. Constant Amplitude

Consider the motion of the i^{th} and $i+1^{th}$ crank as described in the section 2.1.

$$\theta_i = \theta_m \sin(2\pi f t + (i-1)\beta) \tag{13}$$

$$\theta_{i+1} = \theta_m \sin(2\pi f t + i\beta) \tag{14}$$

Where $i = 1, 2, 3, \ldots N$ and N is the number of servo motors used. Simplifying the equation of motion of the adjacent crank angles, (13) and (14) yields (15).

$$\theta_i^2 + \theta_{i+1}^2 - 2\theta_i\theta_{i+1}\cos\beta - \theta_m^2(\sin\beta)^2 = 0 \tag{15}$$

Therefore, a single equation (15) describes the relationship between any two adjacent crank angles in the mechanism. It can be noted that the curve is independent of the frequency of oscillation of the fin and i. Hence, for a constant θ_m and β, the same curve represents the joint angle trajectories of all the adjacent cranks.

4.1.1. Nature of the Curve

The equation (15) is that of a general second degree equation as represented by (5). Here $\Delta = -\theta_m^2 (\sin\beta)^2 \neq 0$ and $D = -(\sin\beta)^2 < 0$. Hence, it can be concluded that (15) represents the equation of an ellipse if $\beta \neq 0, \pi$ and it represents a pair of straight lines if $\beta = 0$ or π.

4.1.2. Standard Form of Ellipse

Equation (15) represents a family of ellipses inclined to the axes for $\beta \neq 0, \pi$. Following the similar steps as discussed in 3.1.3, the standard equation of the ellipse is derived for $0 < \beta < \frac{\pi}{2}$ and $\frac{\pi}{2} < \beta < \pi$, as given by (16) and (17), respectively.

$$\frac{x^2}{\left(\frac{\theta_m \sin\beta}{\sqrt{1-\cos\beta}}\right)^2} + \frac{y^2}{\left(\frac{\theta_m \sin\beta}{\sqrt{1+\cos\beta}}\right)^2} = 1 \quad (16)$$

$$\frac{x^2}{\left(\frac{\theta_m \sin\beta}{\sqrt{1+\cos\beta}}\right)^2} + \frac{y^2}{\left(\frac{\theta_m \sin\beta}{\sqrt{1-\cos\beta}}\right)^2} = 1 \quad (17)$$

Equation (16) represents the standard form of the ellipse with its major axis inclined at 45^0 to the θ_i axis, and equation (17) corresponds to an ellipse with its major axis inclined at -45^0 to the θ_i axis. The axes of the family of ellipses are the same, except that the major axis of (16) is the minor axis of (17) and vice versa. The ellipse becomes a circle for $\beta = \frac{\pi}{2}$.

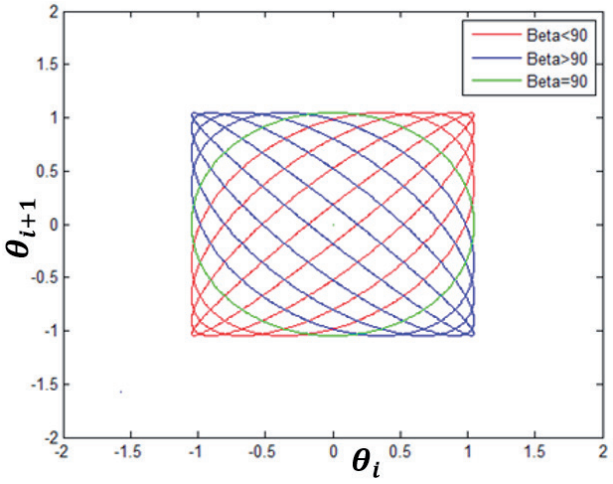

Fig. 9. Bounding square for constant amplitude wave

4.1.3. Area Enclosed by the Ellipse

The area enclosed by an ellipse is $A = \pi ab$ and is given by (18), where a and b are the half lengths of major and minor axis of the ellipse.

$$A = \pi\left(\frac{\theta_m \sin\beta}{\sqrt{1-\cos\beta}}\right)\left(\frac{\theta_m \sin\beta}{\sqrt{1+\cos\beta}}\right) = \pi{\theta_m}^2 \sin\beta \quad (18)$$

4.1.4. Bounding Square

Sum of squares of major and minor axis of the ellipse represented by (16) yield a constant value of $8{\theta_m}^2$ which is independent of β. Therefore, it can be concluded that for a constant θ_m the lengths of the major and minor axis of the ellipse lies on a circle with radius $2\sqrt{2}\theta_m$. This special property of the family of ellipses bounds the length of major and minor axes of the ellipses. The result can be visualized as a growing ellipse with major axis inclined 45^0 to the horizontal. As the β increases, the length of major axis decreases and the length of minor axis increases such that both fall on the circle. To inspect on the bounding nature of all the ellipses, the tangent to the family of ellipses were studied.

$$\frac{\partial\theta_{i+1}}{\partial\theta_i} = \frac{\theta_{i+1}\cos\beta - \theta_i}{\theta_{i+1} - \theta_i\cos\beta} \quad (19)$$

The points on the ellipse having tangents parallel to the θ_i axis are $(\theta_m\cos\beta, \theta_m)$ and $(-\theta_m\cos\beta, -\theta_m)$ is evaluated from the slope of the ellipse given by (19). Hence, a common tangent to all the ellipse exists, which is parallel to the θ_i axis. The common tangent is independent of β and is represented as $\theta_{i+1} = \theta_m$ and $\theta_{i+1} = -\theta_m$. Similarly, the points on the ellipse having tangents perpendicular to the θ_i axis are $(\theta_m, \theta_m\cos\beta)$ and $(-\theta_m, -\theta_m\cos\beta)$. Therefore, the common tangent is $\theta_i = \theta_m$ and $\theta_i = -\theta_m$ and is independent of β. Hence, it can be concluded that all the ellipses have four common tangents which is independent of β. Therefore, the family of ellipses are bounded inside a square of length $2\theta_m$ with (0, 0) as the centre. Fig. 9. and Fig. 10. demonstrate the result.

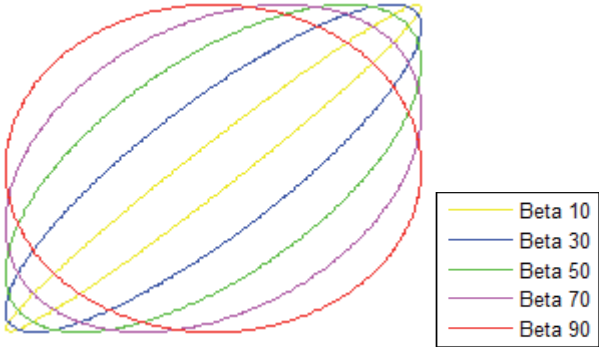

Fig. 10. Joint trajectories for various β

4.2 Linearly Increasing Amplitude

Consider the fin to be operated with a linearly increasing wave described for the i^{th} and $(i+1)^{th}$ cranks as described by (20) and (21).

$$\theta_i = i\,\theta_m \sin(2\pi f t + (i-1)\beta) \quad (20)$$

$$\theta_{i+1} = (i+1)\,\theta_m \sin(2\pi f t + i\beta) \quad (21)$$

Where i=1, 2, 3,...N and N is the number of servo motors used. On simplification, it yields equation (22) that describes the joint angle trajectories.

$$\theta_i{}^2\left(1+\frac{1}{i}\right)^2 + {\theta_{i+1}}^2 - 2\theta_i\theta_{i+1}\cos\beta\left(1+\frac{1}{i}\right) - (\theta_m(i+1)\sin\beta)^2 = 0 \quad (22)$$

It represents a family of ellipses and, unlike in the case of constant amplitude wave generation, the equation of the curve is dependent on i. Hence in order to represent the joint angle trajectories of the curves of a linearly increasing amplitude wave, N–1 number of equations are necessary, as shown in Fig. 12.

4.2.1. Nature of the Curve

The equation (22) is that of a general second degree equation as represented by (5). Hence, Δ and D are evaluated as $\Delta = -(1+i)^4 {\theta_m}^2 (\sin\beta)^4 / i^2$ and $D = -\left(1+\frac{1}{i}\right)^2 (\sin\beta)^2 < 0$. Hence, equation (22) represents an ellipse if $\beta \neq 0, \pi$ and a pair of straight lines if $\beta = 0$ or π.

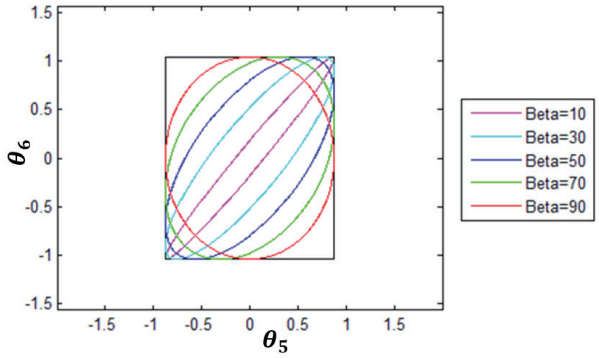

Fig. 11. Bounding rectangle for i=5

4.2.2. Standard Form of the Ellipse

The conversion formula for the ellipses of the form $ax^2 + 2hxy + by^2 + c = 0$, into the general form is given by (23), where $k^2 = 4h^2 + (a-b)^2$.

$$\frac{x^2}{\left(\frac{-2c}{a+b+k}\right)} + \frac{y^2}{\left(\frac{-2c}{a+b-k}\right)} = 1 \tag{23}$$

Hence the standard form of the ellipse representing linearly increasing amplitude is given by (24), where $k^2 = 4(\cos\beta)^2 \left(1+\frac{1}{i}\right)^2 + \left(\left(1+\frac{1}{i}\right)^2 - 1\right)^2$.

$$\frac{x^2}{\left(\frac{2{\theta_m}^2(\sin\beta)^2(i+1)^2}{1+\left(1+\frac{1}{i}\right)^2+k}\right)} + \frac{y^2}{\left(\frac{2{\theta_m}^2(\sin\beta)^2(i+1)^2}{1+\left(1+\frac{1}{i}\right)^2-k}\right)} = 1 \tag{24}$$

Unlike the case of a constant amplitude, the lengths of both major and minor axis are dependent on i and β as demonstrated in Fig. 11. The inclination

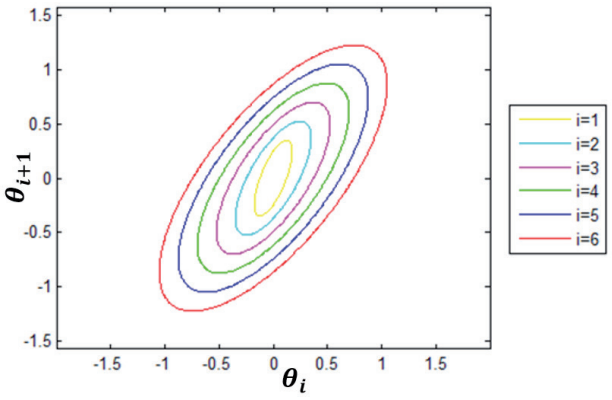

Fig. 12. Joint trajectories for linearly increasing amplitude wave for N=7

α of the minor axis of the ellipse with the θ_i axis is given by (25).

$$\alpha = \frac{1}{2} tan^{-1}\left(\frac{-2\,i(i+1)cos\,\beta}{2i+1}\right) \tag{25}$$

Unlike the case for constant amplitude, the inclination α is not a constant, but is dependent on i and β. The minor axis is along the θ_i axis for $\beta = 0$. The inclination of the ellipse goes on decreasing as i increases for a constant β.

4.2.3. Area Enclosed by the Ellipse

The area enclosed by the ellipse is given by equation (26).

$$A = i(i+1)\pi {\theta_m}^2 \sin\beta \tag{26}$$

4.2.4. Bounding Rectangle

The sum of the squares of major and minor axis of the ellipse represented by (24), is a constant for a particular and is independent of β. Hence, the ellipses are bounded for a particular i, similar to the constant amplitude case. The boundaries are defined by the i value and the boundaries increases as i increases. The points on the ellipse parallel to the θ_i axis are obtained as $(i\theta_m \cos\beta, \theta_m(i+1))$ and $(-i\theta_m \cos\beta, -\theta_m(i+1))$, from the slope of the ellipse represented by equation (27).

$$\frac{\partial\theta_{i+1}}{\partial\theta_i} = \frac{\theta_{i+1}\,cos\,\beta\left(1+\frac{1}{i}\right) - \theta_i\left(1+\frac{1}{i}\right)^2}{\theta_{i+1} - \theta_i\,cos\,\beta\left(1+\frac{1}{i}\right)} \tag{27}$$

Hence the common tangents are $\theta_{i+1} = \theta_m(i+1)$ and $\theta_{i+1} = -\theta_m(i+1)$ and are independent of β. Similarly, the points on the ellipse where the tangents are perpendicular to the θ_i axis are $(i\theta_m, (i+1)\theta_m \cos\beta)$ and $(-i\theta_m, -(i+1)\theta_m \cos\beta)$. Hence, the common tangents are $\theta_i = i\theta_m$ and $\theta_i = -i\theta_m$ which are independent of β. All the four common tangents to the ellipse are independent of β and dependent on i. Therefore, the family of ellipses are bound inside a rectangle when a pair of adjacent cranks are considered, as illustrated in Fig. 11. As the adjacent cranks corresponding to higher amplitude portion of the wave is considered, the size of the bounding rectangle goes on increasing. The size of the bounding rectangle is $2i\theta_m$ by $2(i+1)\theta_m$ centred at origin as shown in Fig. 13.

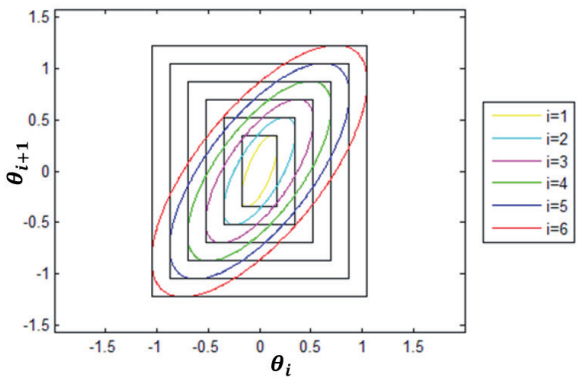

Fig. 13. Increase of size of bounding rectangle with i

5. Feasibility of an Undulation by the Mechanism

Section 3 discusses about the workspace created by a mechanism, while section 4 discusses about the joint trajectory of an undulation. An undulation is said to be feasible only if the joint trajectory completely falls inside the workspace described by the mechanism in [1]. If any portion of the joint trajectory falls out of the workspace, the undulation will remain incomplete in those regions. Therefore, to produce an undulation, the ellipse must be in the region bounded by the C_{min} and C_{max} hyperbolas. For the feasibility of a linearly increasing amplitude wave, the outermost ellipse has to be inside the workspace. Hence, for both waves, the ellipse must be inside the hyperbolas completely. The hydrodynamic effects are not considered in this study.

5.1. Parameters of the Sliders

The minimum and maximum lengths attainable by the slider plays a crucial role in workspace design. Consider that a workspace similar to any one of that of Fig. 7 was chosen, then it is impossible to make an ellipse centered at origin and of any β and θ_m to be in the workspace. Some part of the ellipse will always be outside the workspace. Therefore, a combination of these workspaces have to be adopted. The workspace will accommodate an ellipse only if $C_{min} < L$ and $C_{max} > L$. The length of the slider should be such that it is able to take a length less than L, then extend and cross the length L. For the workspace of Fig. 14, the undulation is impossible. Choosing a slider that can extend to 7 units as shown in Fig. 15, solved the problem.

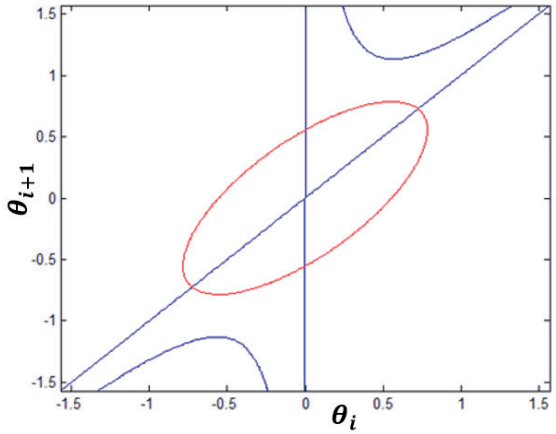

Fig. 14. L = 5, R = 5, C_{min} = 3, C_{max} = 5, β = 45°, θ_m = 45°

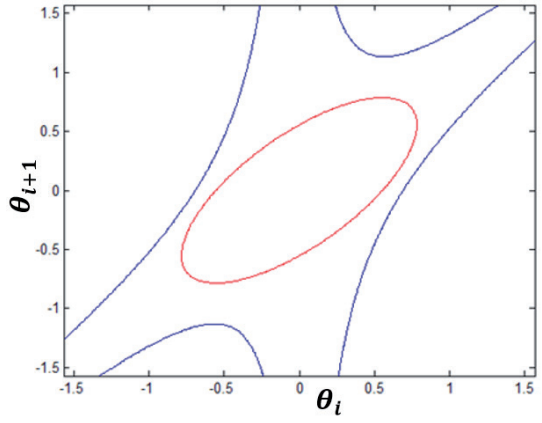

Fig. 15. L = 5, R = 5, C_{min} = 3, C_{max} = 7, β = 45°, θ_m = 45°

5.2. Confirmation of Ellipse Inside Hyperbolas

To have an undulation feasible by the mechanism, any point on the ellipse has to yield a positive sign with the C_{min} hyperbola and a negative sign with the C_{max} hyperbola, given that $C_{min} < L < C_{max}$. Solving equations (12), (13) and (14) for $i = 1$, yield (28) for all values of t.

$$\left(\frac{C_{min}}{R\theta_m}\right)^2 - \left(\frac{L}{R\theta_m}\right)^2 \leq \frac{1}{2}\left[1 + \frac{L}{R}\right] cos\, 4\pi ft + \frac{1}{2}\left[1 - \frac{L}{R}\right] cos[4\pi ft + 2\beta] - cos[4\pi ft + \beta] + cos\,\beta - 1 \leq \left(\frac{C_{max}}{R\theta_m}\right)^2 - \left(\frac{L}{R\theta_m}\right)^2 \quad (28)$$

The equality condition of the equation (28) yields the intersection point of the ellipse and the hyperbola. Hence, the condition (28) should be checked prior to the wave generation using the mechanism.

5.3. Optimal and Feasible Workspace Design

To design an optimal mechanism that can generate a given wave, it is necessary to find the hyperbola touching the ellipse. This optimal solution will ensure that the capability of the membrane to stretch, is fully utilized in generating the wave as shown in Fig. 16. It eliminates the wastage in useful workspace by finding the best fitting hyperbola. The objective function for workspace optimization of a given wave is the minimum distance between the ellipse and hyperbola, which is to be minimized. Since both the curves are inclined with respect to the horizontal at different angles, both the equations (4) and (15) are difficult to solve. It urges the necessity for an optimization algorithm to solve the equations.

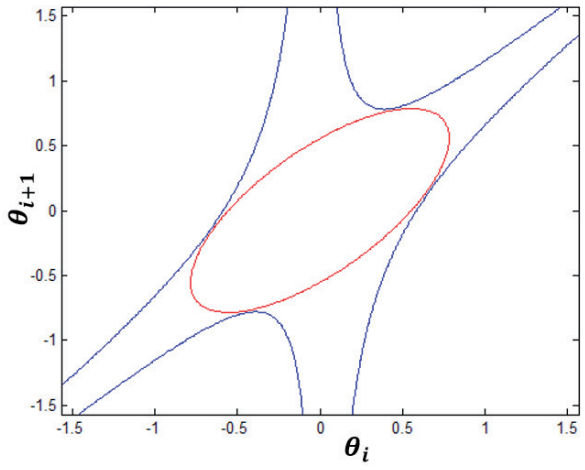

Fig. 16. Optimal mechanism design for β = 45°, θ_m = 45°

6. Conclusion and Outlook

The mathematical modelling of the fins subjected to the mechanical constraint offered by the sliders was done. The effect of the parameter selection of the fin mechanism on the total available workspace was studied in light of the types of undulations that the robot is supposed to take. The feasibility of an undulation by the fin is modelled mathematically. The nature

of the curves representing the constraints and the undulation were studied for optimizing the available workspace.

The analysis begins with the Taylor series approximation for simplification of the equation representing the mechanical constraint offered by the sliders. Error due to this approximation remains throughout the analysis. The feasibility study was done without considering any hydrodynamic effects.

An algorithm to optimize the objective function is to be proposed to reduce the computational complexity in solving the two second degree equations, with both the curves touching each other. The efficiency of the fin mechanism to incorporate more number of undulations should be defined such that it precisely reflects the robot's maneuverability. The wave corresponding to the maximum thrust generation is to be found and incorporated in the workspace. Energy efficiency of the fin is to be evaluated to check for its better performance than thrusters. Further, this technology can be incorporated in the marine drives, as it is expected to be more energy efficient than the thrusters. Future underwater robots can be made with Median Paired Fin Propulsion System, and can be employed for oceanographic researches, underwater surveillance, deep sea mining, swarm robotics etc.

ACKNOWLEDGMENT

This research was supported by National Institute of Technology Calicut, Kerala, India by providing the laboratory facilities and funds for fabrication and experimentation of the robot. This support is gratefully acknowledged.

AUTHORS

Ajith Anil Meera* – Robotics Interest Group, Department of Mechanical Engineering, National Institute of Technology, Calicut, Kerala, India-673601.
Tel. +918547267258.
E-mail: ajitham1994@gmail.com.

Attadappa Puthanveetil Sudheer – Department of Mechanical Engineering Robotics\Mechatronics Lab National Institute of Technology, Calicut Kerala, India-673601
Tel. +919961450987
E-mail: apsudheer@nitc.ac.in

*Corresponding author

REFERENCES

[1] Low K.H, Willy A., "Biomimetic Motion Planning of an Undulating Robotic Fish Fin", *Journal of Vibration and Control*, 2006, vol. 12, no. 12, 1337–1359. DOI: 10.1177/1077546306070597.

[2] Wang S., Dong X., Shang L.-J., et al., "Design and Kinetic Analysis of a Biomimetic Underwater Vehicle with Two Undulating Long-fins", *Acta Automatica Sinica*, 2013, vol. 39, no. 8, 1330–1338. DOI: 10.1016/S1874-1029(13)60049-X.

[3] Sugimori S., Miki H., Yamamoto R., et al., "Braking Performance of a Biomimetic Squid-Like Underwater Robot", *Japan Journal of Bionic Engineering*, 2013, vol. 10, no. 3, 265–273. DOI: 10.1016/S1672-6529(13)60222-X.

[4] Low K.H., "Modelling and parametric study of modular undulating fin rays", *Mechanism and Machine Theory*, 2009, vol. 44, no. 3, 615–632. DOI: 10.1109/ICMA.2007.4303527.

[5] Morawski M., Malec M., Szymak P., Trzmiel A., "Analysis of Parameters of Traveling Wave Impact on the Speed of Biomimetic Underwater Vehicle", *Solid State Phenomena*, vol. 210, 273–279, Oct. 2013, DOI: 10.4028/www.scientific.net/SSP.210.273.

[6] Curet O. M., Lauder G.V., MacIver M.A., Ruiz-Torres R., "Kinematics of the ribbon fin in hovering and swimming of the electric ghost knifefish", *Journal of Experimental Biology*, 2012, vol. 216, no. 5, 823–834. DOI: 10.1242/jeb.076471.

[7] Bale R., Pal A., Bhalla S., et al., "Undulating fins produce off-axis thrust and flow structures", *Journal of Experimental Biology*, 2014, vol. 217, no. 2, pp. 201–213. DOI: 10.1242/jeb.091520

[8] Curet O.M., Neelesh A. Patankar, and M.A. MacIver Anup A. Shirgaonkar, "The hydrodynamics of ribbon-fin propulsion during impulsive motion", *Journal of Experimental Biology*, 2008, vol. 211, no. 21, pp. 3490–3503. DOI: 10.1242/jeb.019224.

[9] Patankar N.A., Lauder G.V., MacIver M.A., Curet O.M., "Aquatic manoeuvering with counter-propagating waves: a novel locomotive strategy", *Journal of Royal Society Interface*, 2010, vol. 8, no. 60, 1041–1050. DOI: 10.1098/rsif.2010.0493

[10] Nevelnb I.D., Rothc E., Mitchelld T.R.T., et al., "Mutually opposing forces during locomotion can eliminate the tradeoff between maneuverability and stability", PNAS, 2013, vol. 110, no. 47, 18798–18803. DOI: 10.1073/pnas.1309300110.